Using Skew Gabor Filter in Source Signal Separation and Local Spectral Multi-Orientation Analysis

Weichuan Yu[1]
[1] Dept. of Diagnostic Radiology
Yale University

Gerald Sommer[2]
[2]Institut für Informatik
Universität Kiel

Kostas Daniilidis[3]
[3]GRASP Laboratory
University of Pennsylvania

Abstract

Responses of Gabor wavelets in the mid-frequency space build a local spectral representation scheme with optimal properties regarding the time-frequency uncertainty principle. However, when using Gabor wavelets we observe a skewness in the mid-frequency space caused by the unsymmetrically spreading effect of Gabor wavelets. Though in most current applications the skewness does not obstruct the sampling of the spectral domain, it affects the identification and separation of source signals from the filter response in the mid-frequency space. In this paper, we present a modification of the original Gabor filter, the skew Gabor filter, to correct the skewness so that the filter responses can be described with a sum-of-Gaussians model. The correction enables us to use higher-order-moment information to analytically separate different source signal components. This provides us with an analytical framework to overcome the limited spectral resolution of other local spectral representations. Examples in source signal separation and local spectral multi-orientation analysis are shown.

1 Introduction

In this paper, we focus on the local spectral analysis. A filter's localization ability is measured by its support. For local signal/image analysis, a narrow filter support is desired both in the spatial domain and in the spectral domain. However, there is a limit in improving the joint localization ability according to the well known uncertainty principle. Because Gabor filters [6] can achieve such a lower bound they are widely used in many spectral analysis tasks such as image representation (e.g. [11]) and the spatio-temporal analysis of motions in image sequences (e.g. [1, 8]). In the spatio-temporal models for motion estimation [1, 2], for example, the energy spectrum of a constant translational motion can be characterized as an oriented plane passing through the origin in the spectral domain. Sampling the spectrum with a set of Gabor filters at different frequencies and orientations [8] may help us to estimate the orientation of the spectral plane. Grzywacz and Yuille [7] further argued that the spectral support of a Gabor filter is a measure of uncertainty and the angle between two tangential lines of the support (which pass through the spectral origin) represents the uncertainty of orientation estimation. This angle is desired to be the same for filters at different frequencies, requiring the spectral support of the filter to be proportional to the distance between the origin and the support center, which is exactly the property of Gabor wavelets.

In applying Gabor wavelets, we observe a positive skewness in the mid-frequency space [7], which is caused by the unsymmetrically spreading effect of Gabor wavelets. The spreading effect and the skewness did not draw considerable attention in the computer vision community because most applications of Gabor wavelets are classification tasks. It is worth mentioning, however, that the filter response in the mid-frequency space (we call this local spectral representation the *mid-spectrum*) blurs the original local spectrum. Consequently, frequency-based approaches often suffer from the coarser resolution. For example, Gabor filters fail to recover the orientation of the well-known multiple motion planes in the spectral domain [2] in multiple motion analysis. In oder to improve the resolution and even recover the original signals, deblurring techniques have been developed, which usually assume symmetric blurring of the original signals. Important applications of deblurring techniques include source signal separation and multiple spectral orientation analysis. Obviously, the skewness in applying Gabor wavelets does not fit the above symmetry assumption and makes deblurring more difficult.

This limitation motivates us to correct the skewness in the mid-spectrum. The correction facilitates the deblurring of filter responses so that we may overcome the limited resolution of frequency-based approaches. In section 2, we shall study the skewness in detail. In section 3, we propose a new filter to correct the skewness. Then, we further describe the corrected mid-spectrum with a sum-of-Gaussians model and use higher-order-moment information to identify different source signals in section 4. The issue of multi-orientation analysis will be addressed in section 5 with experimental examples. This paper is concluded in section 6.

2   The Skewness of Gabor Wavelets

We first study the positive skewness in applying Gabor wavelets. For simplicity we begin with a 1-D Gabor filter whose impulse response reads

$$g_1(x; \omega_0, \sigma_x) = \frac{1}{\sqrt{2\pi}\sigma_x} \, e^{-\frac{x^2}{2\sigma_x^2}} \, e^{j\omega_0 x}. \qquad (1)$$

Here ω_0 denotes the mid-frequency and σ_x is the scale parameter. The spectrum of $g_1(x; \omega_0, \sigma_x)$ is a Gaussian centered at ω_0

$$G_1(\omega; \omega_0, \sigma_x) = e^{-\frac{\sigma_x^2(\omega-\omega_0)^2}{2}} \qquad (2)$$

with bandwidth inversely proportional to σ_x. In local signal analysis, we usually calculate the spatial convolution between $g_1(x; \omega_0, \sigma_x)$ and the signal $i(x)$, yielding

$$h_1(x; \omega_0, \sigma_x) = \int_{\xi=-\infty}^{\infty} i(\xi) g_1(x - \xi) d\xi. \qquad (3)$$

At a fixed position x_0, the filter response is simplified as an inner product

$$h_1(x_0; \omega_0, \sigma_x) = \int_{\xi=-\infty}^{\infty} i(\xi) g_1(x_0 - \xi) d\xi. \qquad (4)$$

Here the Gaussian envelope of $g_1(x)$ defines the local neighborhood, although $d\xi$ still goes from $-\infty$ to ∞. Using the Parseval theorem ([4], pp.113-115) and the facts that $g_1(x_0 - x) = g_1^\star(x - x_0)$ and $G_1^\star(\omega) = G_1(\omega)$ (here $\star$ denotes conjugation), the above inner product can also be represented in the spectral domain as follows

$$h_1(x_0; \omega_0, \sigma_x) = \int_{\omega=-\infty}^{\infty} I(\omega) G_1(\omega) e^{j\omega x_0} d\omega. \qquad (5)$$

Here $I(\omega)$ is the spectrum of $i(x)$. Thus, at $x = x_0$ (for simplicity we may set $x_0 = 0$) we obtain a local spectral representation of the original signal, which is a function of the mid-frequency ω_0 and the scale σ_x. We call this local spectral representation the *mid-spectrum*.

The mid-spectrum $h_1(\omega_0, \sigma_x)$ spreads every spectral Dirac component of the source signal into a function of ω_0 and therefore blurs the spectrum of the source signal. Assume that the spectrum of the source signal is a Dirac function $I(\omega) = \delta(\omega - \omega_i)$ originating from a complex harmonic. Its mid-spectrum turns out to be

$$h_1(\omega_0, \sigma_x) = G_1(\omega_0; \omega_i, \sigma_x) = e^{-\frac{\sigma_x^2(\omega_0-\omega_i)^2}{2}}. \qquad (6)$$

If the parameter σ_x is a constant like in plain Gabor filters, then $h_1(\omega_0, \sigma_x)$ is a Gaussian spreading of $\delta(\omega - \omega_i)$ and

there is no skewness. However, if the wavelet property is preferred, i.e. σ_x is inversely proportional to ω_0

$$\sigma_x = \frac{C}{\omega_0} \qquad (7)$$

with C as a constant. Then, we observe the positive skewness of ω_0 [7] (see also figure 1)

$$h_1(\omega_0) = e^{-\frac{C^2(\omega_0-\omega_i)^2}{2\omega_0^2}}. \qquad (8)$$

We may straightforwardly extend the above analysis to n-dimensional Gabor wavelets with isotropic envelope. For 2-D Gabor wavelets in the spatio-temporal domain with the following relation

$$\sigma_x = \sigma_t = \frac{C}{\sqrt{\omega_{x0}^2 + \omega_{t0}^2}}, \qquad (9)$$

the mid-spectrum of a 2-D impulse $\delta(\omega_x - \omega_{xi}, \omega_t - \omega_{ti})$ then reads

$$h_2(\omega_{x0}, \omega_{t0}) = e^{-\frac{C^2[(\omega_{x0}-\omega_{xi})^2+(\omega_{t0}-\omega_{ti})^2]}{2(\omega_{x0}^2+\omega_{t0}^2)}}. \qquad (10)$$

Figure 1 displays two skewness examples of 1D- and 2D-Gabor wavelets.
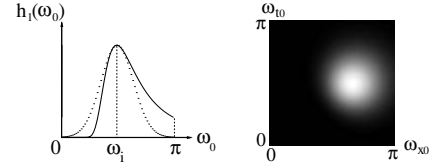
Figure 1: The skewness of Gabor wavelets. **Left:** The solid curve is $h_1(\omega_0)$ in equation (8) and the dotted curve is a Gaussian function centered at ω_i with the scale parameter $\frac{\omega_i}{C}$. $C = 3.5, \omega_i = \frac{\pi}{2}$. **Right:** 2-D skewness $h_2(\omega_{x0}, \omega_{t0})$ in equation (10). White pixels denote large values. $C = 3.5, \omega_{xi} = \frac{2\pi}{3}, \omega_{ti} = \frac{\pi}{2}$. In both cases, Gabor wavelets blur the input Dirac function into a widely-spreading function.

In many Gabor wavelets approaches (e.g. [10, 12]), this skewness is harmless because it does not obstruct the descriptions of different signals with a set of samples. Thus, the main attention was attracted to the efficient covering/sampling of the spectrum as well as the coefficient estimation of the Gabor basis [3, 11]. But we should keep in mind that Gabor wavelets really blur the input signal in the mid-frequency space. As a result, the spectral resolution in the mid-spectrum is much worse than that in the original signal. More importantly, the non-symmetric blurring in the Gabor wavelets further hampers the possible application of deblurring techniques, which work well only under

the assumption of symmetric blurring. In order to apply de-blurring techniques in the mid-spectrum and eventually use the mid-spectrum in source signal separation and multiple-orientation analysis, we need to correct the skewness in Gabor wavelets.

3 Skew Gabor Filter

In order to correct the skewness, we design a new *skew Gabor filter* whose spectral definition reads

$$SG_1(\omega; \omega_0, C) = \exp\{-\frac{C^2(\omega - \omega_0)^2}{2\,\omega^2}\}. \quad (11)$$

For a source signal whose spectrum is a Dirac function $I(\omega) = \delta(\omega - \omega_i)$, the mid-spectrum after skew Gabor filtering is an ideal Gaussian

$$sh_1(\omega_0, C) = \exp\{-\frac{C^2(\omega_0 - \omega_i)^2}{2\,\omega_i^2}\}. \quad (12)$$

The symmetry in the mid-spectrum is therefore achieved using the new filter.

The spectral shape of the skew Gabor filter, especially the tail of the filter depends very much on the value of C:

$$\lim_{\omega \to \infty} SG_1(\omega; \omega_0, C) = e^{-\frac{C^2}{2}}. \quad (13)$$

Figure 2 shows clearly that larger C values make the tail of the filter closer to zero, which means that the filter is more likely to have finite energy in the spectral domain. Thus, a large C value is preferred in order to simplify the application of the Fourier theory. On the other hand, however, a large C value also needs large filter kernel in the spatial domain. Obviously, the filter kernel could not be arbitrarily large in many local image analysis applications. In this paper, we choose $C = 3.5$ so that the filter kernel has a reasonable size in the spatial domain. Also, its energy in the spectral domain is approximately finite since the amplitude of $e^{-\frac{C^2}{2}}$ with $C = 3.5$ is about 0.22% of the maximal spectral amplitude of the filter at ω_0 and can be considered as approximately negligible.
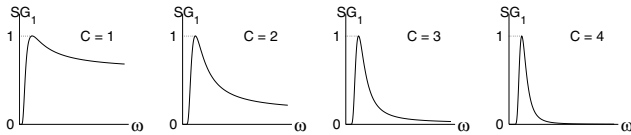
Figure 2: Spectra of skew Gabor filters with different C values. With $C \geq 3$, $\lim_{\omega \to \infty} SG_1(\omega; \omega_0, C)$ is close to zero. $\omega_0 = \frac{\pi}{2}$.

The skew Gabor filter in the spatial domain $sg_1(x)$ has no analytical expression because there is no closed-form representation of the inverse Fourier transform of $SG_1(\omega)$. We

may obtain an FIR version of both the real and the imaginary part of $sg_1(x)$ using an FIR window in the Fourier domain and inverse discrete Fourier transform (DFT). One example of the skew Gabor filter in the spatial domain is shown in figure 3. Although the skew Gabor filter decays slower than the Gabor filter, the energy primarily lies inside the central part of the Gaussian envelope (i.e. between -12 and 12 on the left side in figure 3). If we extract the central part of the plot as an FIR filter, the energy loss is negligible.
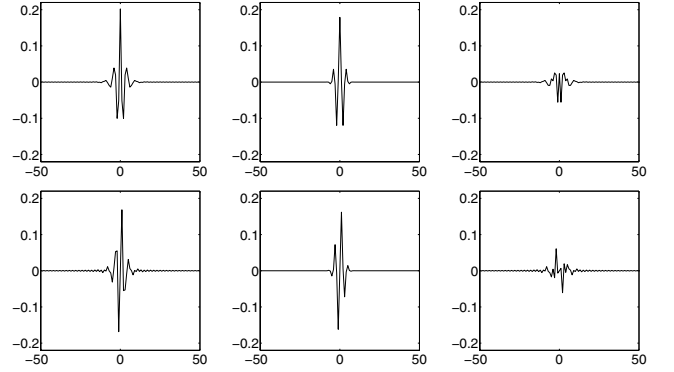
Figure 3: **Top:** The real parts of a 1-D skew Gabor filter (left) and a Gabor filter (middle) as well as their even-symmetric difference (right). **Bottom:** The imaginary parts of both filters (left: skew Gabor; middle: Gabor) and their odd-symmetric difference (right). The parameters are $C = 3.5$ and $\omega_0 = \frac{\pi}{2}$.

Similarly, we may correct the skewness of 2-D Gabor wavelets by using a 2-D skew Gabor filter

$$SG_2(\omega_x, \omega_t) = e^{-\frac{C^2[(\omega_x - \omega_{x0})^2 + (\omega_t - \omega_{t0})^2]}{2(\omega_x^2 + \omega_t^2)}}. \quad (14)$$

The mid-spectrum corresponding to $\delta(\omega_x - \omega_{xi}, \omega_t - \omega_{ti})$ is then a 2-D Gaussian centered at $(\omega_{xi}, \omega_{ti})$

$$sh_2(\omega_{x0}, \omega_{t0}, C) = e^{-\frac{C^2[(\omega_{x0} - \omega_{xi})^2 + (\omega_{t0} - \omega_{ti})^2]}{2(\omega_{xi}^2 + \omega_{ti}^2)}}. \quad (15)$$

4 1-D Source Signal Separation

In the following, we demonstrate the merit of correcting the positive skewness. We start with a 1-D source signal separation example by assuming that the spectrum of an input signal is composed of two Dirac components

$$S(\omega) = a_1\delta(\omega - \mu_1) + a_2\delta(\omega - \mu_2), \quad (16)$$

where their amplitudes (a_1 and a_2) and offsets (μ_1 and μ_2) are unknown. Our goal is to estimate these amplitudes and offsets from the mid-spectrum so that the source components can be identified and separated. Here we provide such

a simple example with known parameters to simplify the comparison between Gabor wavelets and skew Gabor filters. Our focus is the comparison between two different local spectral analysis methods. Certainly the traditional Fourier analysis can easily deal with such a simple spectrum. But the traditional Fourier transform also has to face the poor localization ability in the spatial domain, aliasing problem in the sampling, and block effect in extracting a Fourier window. Actually, it was these problems that make the local spectral analysis methods attractive since they provide solutions to these problems.

When we apply plain Gabor wavelets for filtering, the mid-spectrum is an overlap of two skewness curves (cf. equation (8)) and it is very hard to detect the source signals by directly searching for the local maxima (cf. figure 4). Though iterative algorithms (e.g. [13]) or learning methods (e.g. [5]) may be used to extract the desired parameters, such non-analytic approaches are computationally inefficient and are sensitive to initial values and related parameters in the cost function. Besides, they are susceptible to local minima in the regression procedure. Thus, we prefer to use an analytic framework for parameter regression.

The correction of skewness makes this idea possible. Under the same assumption as that in equation (16), the mid-spectrum of skew Gabor filters is then a sum of two differently weighted and shifted Gaussian functions (for simplicity we omit the coefficient term $\frac{1}{\sqrt{2\pi}\sigma}$ of Gaussian)

$$g(\omega_0) = g_1(\omega_0) + g_2(\omega_0) \qquad (17)$$

with

$$\begin{cases} g_1(\omega_0) &= a_1 e^{-\frac{(\omega_0-\mu_1)^2}{2(\frac{\mu_1}{C})^2}} \\ g_2(\omega_0) &= a_2 e^{-\frac{(\omega_0-\mu_2)^2}{2(\frac{\mu_2}{C})^2}} \end{cases} . \qquad (18)$$

The scale parameters in above Gaussians are proportional to the mean values. In figure 5 we demonstrate the mid-spectrum of plain Gabor wavelet filtering as well as the mid-spectrum of skew Gabor filtering.

The sum-of-Gaussians model is well studied from statistic aspect and is widely used in neural network approaches (e.g. [13]). One benefit of this model is that we are able to use higher-order moment information to extract parameters. The calculation of the moments leads to the following system of equations in a_1, a_2, μ_1, and μ_2

$$\begin{cases} a_1\mu_1 + a_2\mu_2 &= m_0\frac{C}{\sqrt{2\pi}} &= b_1 \\ a_1\mu_1^2 + a_2\mu_2^2 &= m_1b_1 &= b_2 \\ a_1\mu_1^3 + a_2\mu_2^3 &= \frac{1}{\frac{1}{C^2}+1}m_2b_1 &= b_3 \\ a_1\mu_1^4 + a_2\mu_2^4 &= \frac{1}{\frac{3}{C^2}+1}m_3b_1 &= b_4 \end{cases} . \qquad (19)$$
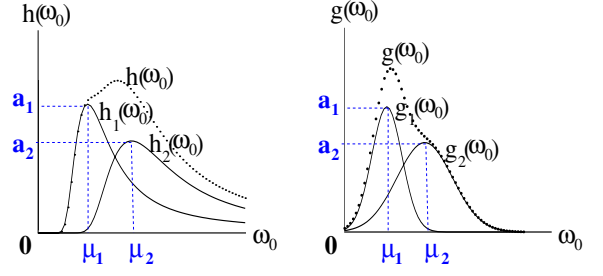
Figure 4: **Left:** The mid-spectrum of plain Gabor wavelet filtering. **Right:** The superposition of two Gaussians after 1-D skew Gabor filtering. The scale parameters of these two Gaussians are determined by $\frac{\mu_1}{C}$ and $\frac{\mu_2}{C}$, respectively.

Here m_0 denotes the integration of $g(\omega_0)$ and m_1, m_2, and m_3 denote the first three order moments of $g(\omega_0)/m_0$. Without loss of generality we assume $0 < \mu_1 \leq \mu_2$. Solving these equations yields

$$\begin{cases} a_1 &= \frac{a(2ab_2+bb_1+b_1\sqrt{b^2-4ac})}{b^2-4ac-b\sqrt{b^2-4ac}} \\ a_2 &= \frac{a(2ab_2+bb_1-b_1\sqrt{b^2-4ac})}{b^2-4ac+b\sqrt{b^2-4ac}} \\ \mu_1 &= \frac{-b+\sqrt{b^2-4ac}}{2a} \\ \mu_2 &= \frac{-b-\sqrt{b^2-4ac}}{2a} \end{cases} , \qquad (20)$$

where the variables a, b, and c are defined as

$$\begin{cases} a &= (b_2)^2 - b_1b_3 \\ b &= b_1b_4 - b_2b_3 \\ c &= (b_3)^2 - b_2b_4 \end{cases} . \qquad (21)$$

Here real solutions are guaranteed since the discriminator is always not less than zero

$$b^2 - 4ac = [a_1a_2\mu_1\mu_2(\mu_1-\mu_2)^3]^2 \geq 0 \qquad (22)$$

If $b^2 - 4ac = 0$, there is only one single Gaussian (i.e. $\mu_1 = \mu_2$) and we can simply estimate its mean value and amplitude from the first two equations in (19).

In figure 5 we display an example of source signal separation. The input signal is composed of two cosine functions

$$s(x) = 2\cos(\frac{\pi}{4}x) + \cos(\frac{3\pi}{8}x) \qquad (23)$$

with the spectrum $S(\omega) = \delta(\omega \pm \frac{\pi}{4}) + \frac{1}{2}\delta(\omega \pm \frac{3\pi}{8})$. Now we sample the positive spectral space with Gabor wavelets and skew Gabor filters. We start the mid-frequency at $\omega_0 = \frac{\pi}{128}$ and increase it with a step of $\frac{\pi}{128}$ to get a dense sampling. Here we set the highest mid-frequency as $\omega_0 = \frac{7\pi}{8}$ so that we do not need to consider the boundaries in the mid-spectrum. Although the spectrum of the input signal is a simple sum of two Dirac functions, the mid-spectra using both filters are so blurred that it is hard to identify the source
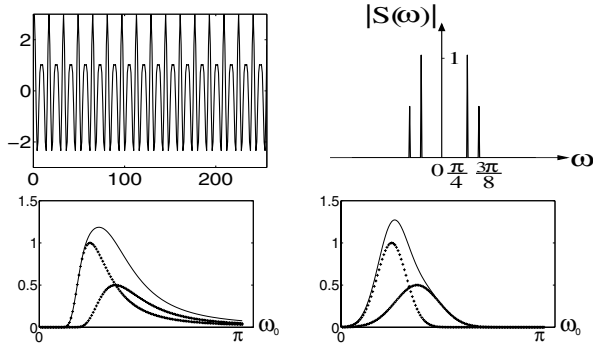
Figure 5: **Top:** The source signal and its energy spectrum. **Bottom:** The positive mid-spectra (solid lines) using plain Gabor wavelets (left) and using skew Gabor filters (right). These curves are actually overlapping of the spreading responses of two Dirac functions (shown as crosses).

signals by direct observation (see figure 5). The positive skewness in applying Gabor wavelets even makes it impossible to apply deblurring methods. In contrast, after correcting the skewness we can estimate the amplitudes and the locations of two positive Dirac components analytically using higher order moment information (cf. equation (20)). The estimation results are very close to the true values (see table 1). For comparison, we also extract higher order moment information blindly from the mid-spectrum after Gabor wavelets filtering and use equation (20) again for estimation. As the sum-of-Gaussians model is no more valid, the estimation results are far away from the true values, as shown in table 1 as well.

Parameter	True Value	GW	SG
a_1	1	1.1451	0.9976
a_2	0.5	0.2870	0.4825
μ_1	$\pi/4 = 0.7854$	1.0814	0.8130
μ_2	$3\pi/8 = 1.1781$	1.7965	1.2079

Table 1: Estimation results using Gabor wavelets (GW) and skew Gabor filters (SG). For comparison we apply the same higher-order-moment framework on the mid-spectra.

In the negative frequencies, we may perform a similar procedure to extract the desired parameters. Then, we are able to identify the source signal components in spite of the blurring in the mid-spectrum. In other words, this method can "deblur" the mid-spectrum. Taking into account that a lot of efforts had to be made in filter design so that the blurring after filtering does not significantly affect the identification of signals or orientations (e.g. [15]), this framework provides an analytical solution to improve the spectral resolution.

5   Local Spectral Multi-Orientation Analysis

In this section, we analyze the appearance of multiple orientations in 2-D spectral space. This has applications in multiple motion analysis. It is known that both 1-D occlusion and 1-D transparency may be modeled as multiple lines in the spectral domain, with some distortion in case of occlusion and without distortion in case of transparency. Thus, the problem of motion estimation turns out to be an issue of orientation analysis in the spatio-temporal space. As the angle between two spectral lines can be arbitrary, eigen-analysis (e.g. [14, 9]) cannot properly determine the orientation of multiple lines. Sampling the spectrum with Gabor filters [8] provided a good motivation, but suffered under the limited resolution. Here we prove that this limitation may be overcome using skew Gabor filters.

The main point here is to study the angular distribution of the energy spectrum. For two spectral lines passing through the origin, the polar integration of the spectral lines along the radial direction yields the sum of two Dirac components in the angular space, which reminds us the similarity between 2-D orientation analysis and 1-D source signal separation. In fact, the mid-spectrum after 2-D skew Gabor filtering consists of 2-D Gaussians concentrating along the spectral lines — the skewness has been corrected. The remaining question is if the angular distribution of the mid-spectrum can be described as a sum of two Gaussians. To answer this question, let us first study the angular distribution of one 2-D Gaussian.

For a 2-D Gaussian centered at $O_i = (\omega_{xi}, \omega_{ti})$ (cf. figure 6), its angular distribution after a polar integration reads (here we only show the result due to the space limitation)

$$
\begin{aligned}
sh_a(\theta) = &\frac{1}{2\pi} e^{-\frac{C^2}{2}} + \frac{C}{2\sqrt{2\pi}} \cos(\theta - \theta_i)\, e^{-\frac{C^2 \sin^2(\theta - \theta_i)}{2}} \\
&\cdot [1 + \mathbf{erf}(\frac{C}{\sqrt{2}} \cos(\theta - \theta_i))],
\end{aligned} \tag{24}
$$

where θ_i is the polar angle of the point O_i and $\mathbf{erf}(x)$ is the error integral function defined as

$$
\mathbf{erf}(x) = \frac{2}{\sqrt{\pi}} \int_0^x e^{-t^2} dt.
$$

This expression is rather complicated at a first sight. But it has only one parameter θ and is symmetric with respect to the angle θ_i. Further, the only difference between the polar integration and the marginal integration of a 2-D Gaussian is the integration path: the polar integration paths go along the radial direction, while the marginal integration paths go in a parallel direction. It is known that the marginal integration of a 2-D Gaussian is a 1-D Gaussian. Therefore, it is reasonable to guess that equation (24) can be approx-

imated by a 1-D Gaussian $N(\theta_i, \sigma_a)$, especially when the polar integration paths are close to be parallel.
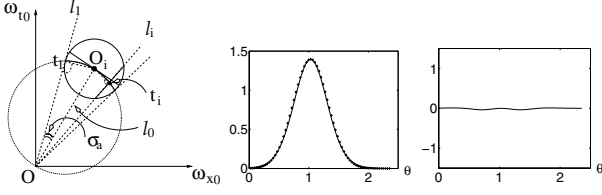
Figure 6: The polar integration of an isotropic Gaussian can be approximated by an ideal Gaussian function $N(\theta_i, \sigma_a)$. **Left:** The solid circle centered at O_i represents the support of the Gaussian. The pencil of lines passing through the origin denotes the integration paths. The middle point of the intersection between a integration path and the solid circle lies on the dotted circle passing through the origin and O_i. **Middle:** The solid curve is the plot of $sh_a(\theta)$ (cf. equation (24)) with $C = 3.5$ and $\theta_i = arctan(\frac{5}{3})$. A Gaussian $N(\theta_i, \sigma_a)$ with $\sigma_a = \sin^{-1}(1/C)$ is plotted with crosses. **Right:** The difference between $sh_a(\theta)$ and $N(\theta_i, \sigma_a)$. The maximal difference is less than 2% of $sh_a(\theta_i)$.

Indeed, the arc variable is a good approximation of the diameter near the point O_i, especially if C is large enough. Mathematically, the relation can be expressed as (cf. figure 6):

$$\sigma_a = sin^{-1}(|r_i| \, / \, |l_0|) = sin^{-1}(1 \, / \, C). \qquad (25)$$

This angle σ_a is an ideal index to describe the approximation error because it indicates the difference between the arc variable and the linear variable. The smaller the σ_a value is, the smaller the approximation error (for the marginal integration with no approximation error, this angle equals to zero). For the example shown in figure 6 with $C = 3.5$, the maximal difference between $sh_a(\theta)$ and $N(\theta_i, \sigma_a)$ is less than 2% of the maximal amplitude of $sh_a(\theta)$ (i.e. $sh_a(\theta_i)$).

Now let us come to the angular distribution of the complete mid-spectrum after 2-D skew Gabor filtering. As the mid-spectrum of two motions is a set of 2-D Gaussians centered on two spectral lines, the polar integration of the mid-spectrum along each spectral line is then a sum of 1-D Gaussians with the same mean value and the same scale parameter σ_a. Consequently, the angular distribution of the mid-spectrum is the superposition of two 1-D Gaussians. Mathematically, the superposition of two angular Gaussians reads

$$g_a(\theta) = a_1 e^{-\frac{(\theta - \mu_1)^2}{2\sigma_a^2}} + a_2 e^{-\frac{(\theta - \mu_2)^2}{2\sigma_a^2}}. \qquad (26)$$

The above equation is very similar to equations (17) and (18) except that the variances of two Gaussians are now constant. Therefore, we can use the same method introduced in section 4 to analytically solve the mean values of

two angular Gaussians. In the following, we will show that it is impossible to apply the analytical framework without correcting the skewness of Gabor wavelets.

5.1 Evaluation Example

To demonstrate the merit of skewness correction, we compare Gabor wavelets and skew Gabor filter using two synthetic examples with known ground truth and one real example. The first example demonstrates the deblurring ability of our framework. We synthesize a 2-D signal whose spectrum is composed of two spectral lines passing through the origin (figure 7). The polar angles of these two lines are 30° and 60°, respectively. The mid-spectra after Gabor wavelets filtering and skew Gabor filtering are both strongly blurred so that the source signals are hardly to recognize in the mid-spectra. For comparison, we apply the same higher-order-moment framework on the polar integration results of both mid-spectra. The estimated polar angles are listed in table 2 together with the true values. Clearly, the results from skew Gabor filtering are closer to the true values than the results from Gabor wavelets filtering.
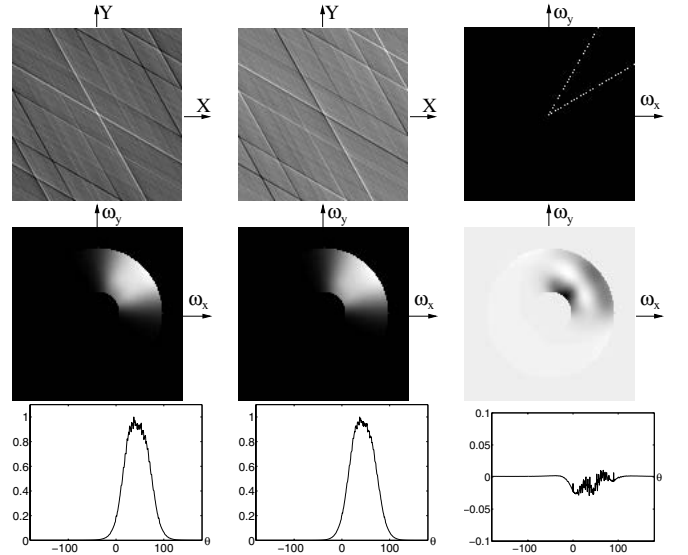
Figure 7: **Row 1:** The real part (left), the imaginary part (middle), and the energy spectrum (right) of a 2-D signal. The polar angles of two lines in the spectrum are 30° and 60°, respectively. **Row 2:** The mid-spectra using 2-D Gabor wavelets (left) and skew Gabor filters (middle) with $C = 3.5$ and their difference (right). The mid-frequency satisfies $\pi/4 \leq \sqrt{\omega_{x0}^2 + \omega_{t0}^2} \leq 3\pi/4$. **Row 3:** Normalized angular distributions of the mid-spectra (left: Gabor wavelets; middle: skew Gabor filter) and their difference (right). Note that the difference image has a smaller scale.

The second example is to estimate motion parameters from

Parameter	True Value	GW	SG
μ_1	30°	11.39°	26.50°
μ_2	60°	55.72°	62.19°

Table 2: Estimation results using Gabor wavelets (GW) and skew Gabor filters (SG).
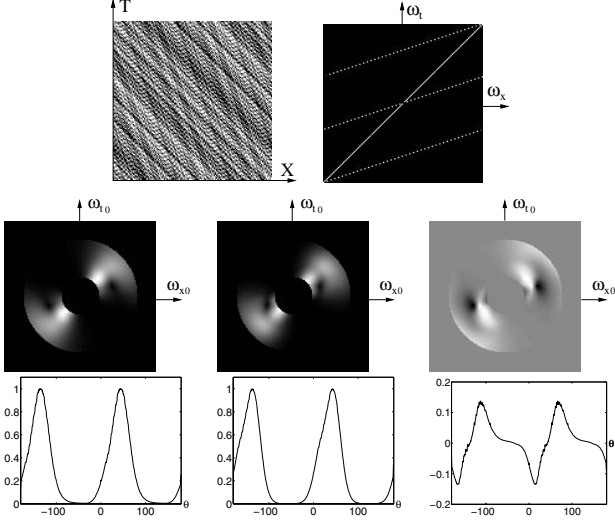
Figure 8: **Row 1:** The 1-D random dot transparency sequence (left) and its energy spectrum after applying DFT directly. The overlapping of two source signals forms oriented structures in the spatial-temporal plane. **Row 2:** The mid-spectra after Gabor wavelets filtering (left) and skew Gabor filtering (middle). Their difference is shown on the right. **Row 3:** The normalized angular distributions corresponding to the mid-spectra and their difference. The estimated polar angles of the spectral lines are listed in table 3.

Parameter	True Value	GW	SG
μ_1	18.43°	26.32°	16.38°
μ_2	45.00°	58.98°	45.74°
$v_1 = cot(\mu_1 - 90°)$	−0.33	−0.49	−0.29
$v_2 = cot(\mu_2 - 90°)$	−1.00	−1.66	−1.03

Table 3: Estimation results in the synthesized transparency sequence using Gabor wavelets (GW) and skew Gabor filters (SG).

a 1-D transparency sequence, which is the simple overlapping of two source signals. We set the velocities of two source signals as −0.33 [pixel/frame] and −1 [pixel/frame], respectively. Correspondingly, the polar angles of two spectral lines are 18.43° and 45.00°. Note that the spatial periodicity of discrete Fourier transform (DFT) cannot be fulfilled for such a non-harmonic image. Consequently, we observe the aliasing effect after applying DFT directly on the original signal, as shown in figure 8. In order to avoid

the aliasing problem, we low-pass the signal before starting the spectral-sampling. Similar to the first example, the mid-spectra after both Gabor wavelets filtering and skew Gabor filtering are displayed in figure 8. After the polar integration of the mid-spectra, we use the higher-order-moment framework to estimate the polar angles of the original spectral lines and further use the equation $v = cot(\mu - 90°)$ to estimate the velocities of the source signals. Table 3 shows clearly that the polar angles of the spectral lines and the estimated velocities after Gabor wavelets filtering are far away from the true values, while skew Gabor filtering provides reasonable results.
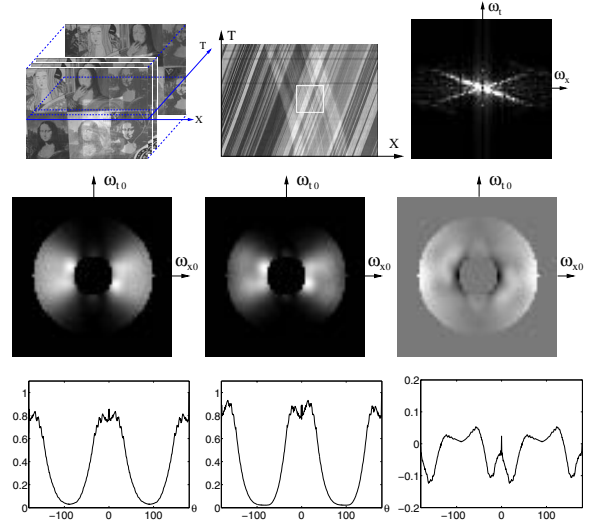
Figure 9: **Row 1 Left:** Extracting an X-T plane from a real transparency sequence. **Row 1 Middle:** The X-T plane in detail. In the white window, two motions are nearly constant. **Row 1 Right:** The energy spectrum of the signal in the white window after direct DFT. The vertical energy bar is not a printing problem. It is caused by the temporal intensity variation in the white window (cf. Row 1 Middle). **Row 2:** The mid-spectra after Gabor wavelets filtering (left) and skew Gabor filtering (middle) and their difference (right). **Row 3:** Normalized angular distributions of the mid-spectra and their difference (from left to right).

Figure 9 shows a real transparency sequence consisting of a right-moving portrait and a left-moving package mirrored on the frame of the portrait. Since both motions are horizontal, we can simplify the problem of motion estimation by cutting an X-T plane through the image sequence. In the X-T plane, we observe two motions as two oriented structures. In the 64×64 white window, we take the DFT directly and obtain the energy spectrum (row 1 right in figure 9). Unlike in the synthetic examples, the ground truth of the motion parameters is unknown. Fortunately, the motions in the white window are almost constant. Thus, we can extract

Parameter	True Value	GW	SG
μ_1	$\approx -20.56°$	$-26.27°$	$-22.97°$
μ_2	$\approx 18.43°$	$26.83°$	$25.29°$
$\mu_2 - \mu_1$	$38.99°$	$53.10°$	$48.26°$
v_1	≈ 0.37	0.49	0.42
v_2	≈ -0.33	-0.51	-0.47

Table 4: Measured and estimated parameter values in the real transparency sequence. The results using skew Gabor filtering (SG) are closer to the measured values than the results using Gabor wavelets filtering (GW).

the motion parameters roughly by measuring the structure orientation.

Table 4 shows that the skew Gabor filter provides results closer to the measured values than Gabor wavelets. The difference between the skew Gabor filter and Gabor wavelets is not as significant as the difference in the random dot transparency example. This is partially due to the fact that the visible energy components outside the spectral lines bias the sum-of-Gaussians model (There are energy components lying horizontally and vertically outside the spectral lines due to the aliasing effect, noise, and temporal variation of intensity). More importantly, the spectral lines in the energy spectrum happen to be nearly symmetric about the ω_x-axis. As the skewness of each spectral line after Gabor wavelets filtering (cf. equation (10)) appears along the direction leaving the ω_{x0}-axis, the skewness in the mid-spectrum has been partially compensated due to the symmetric properties of the spectral lines (This analysis can be proved by the angular distribution of the mid-spectrum in figure 9). Consequently, the mid-spectrum after Gabor wavelets filtering is closer to the sum-of-Gaussians model.

6 Conclusion and Future Work

In this paper, we have proposed a new filter to correct the skewness of Gabor wavelets in the mid-frequency space. After the correction, we are able to model the distribution in the parameter space with a sum-of-Gaussians model. We then use a higher-order-moment framework to analytically separate **two** source signals in 1-D space and in 2-D angular space.

The application examples in this paper are very simple. We have limited the number of Gaussians to be no more than two and we have not considered noise in the higher-order-moment framework. We have not shown how to extend the current framework to the 3-D spatial-temporal space to analyze multiple motions in the real world, in which the spectral lines turn out to be spectral planes. These issues certainly need to be addressed before we can apply

the higher-order-moment framework in more complex applications. Nevertheless, the advantages of correcting the skewness of Gabor wavelets should be recognized: The statistical simplicity of Gaussians is a very attractive property. While describing the spectral distribution analytically is very difficult without correcting the skewness, the use of sum-of-Gaussians model is straightforward after correcting the skewness. It also shows a possible way to *deblur* filtered signals and eventually overcome the limited resolution of spectral representations.

References

[1] E. H. Adelson and J. R. Bergen. Spatiotemporal energy models for the perception of motion. *Journal of Optical Society of America A*, 2(2):284–299, 1985.

[2] S.S. Beauchemin and J.L. Barron. The frequency structure of 1d occluding image signals. *IEEE Trans. Pattern Analysis and Machine Intelligence*, 22:200–206, 2000.

[3] A. C. Bovik, M. Clark, and W. S. Geisler. Multichannel texture analysis using localized spatial filters. *IEEE Trans. Pattern Analysis and Machine Intelligence*, 12(1):55–73, 1990.

[4] R.N. Bracewell. *The Fourier Transform and Its Applications*. McGraw-Hill Book Company, 1986.

[5] J.G. Daugman. Complete discrete 2-d Gabor transforms by neural networks for image analysis and compression. *IEEE Trans. Acoustics, Speech, and Signal Processing*, 36(7), 1988.

[6] D. Gabor. Theory of communication. *Journal of the IEE*, 93:429–457, 1946.

[7] N.M. Grzywacz and A.L. Yuille. A model for the estimate of local image velocity by cells in the visual cortex. *Proc. Royal Society of London.*, B 239:129–161, 1990.

[8] D. J. Heeger. Optical flow using spatiotemporal filters. *International Journal of Computer Vision*, 1(4):279–302, 1988. +

[9] B. Jähne. *Spatio-Temporal Image Processing*. Springer-Verlag, 1993.

[10] A.K. Jain and F. Farrokhnia. Unsupervised texture segmentation using Gabor filters. *Pattern Recognition*, 24(12):1167–1186, 1991.

[11] T. S. Lee. Image representation using 2D Gabor wavelets. *IEEE Trans. Pattern Analysis and Machine Intelligence*, 18(10):959–971, 1996.

[12] B.S. Manjunath and W.Y. Ma. Texture features for browsing and retrieval of image data. *IEEE Trans. Pattern Analysis and Machine Intelligence*, 18(8):837–842, 1996.

[13] T. Poggio and F. Girosi. Networks for approximatation and learning. *Proceedings of the IEEE*, 78(9):1481–1497, 1990.

[14] M. Shizawa and K. Mase. A unified computational theory for motion transparency and motion boundaries based on eigenenergy analysis. In *IEEE CVPR*, pages 289–295, 1991.

[15] E. P. Simoncelli and H. Farid. Steerable wedge filters for local orientation analysis. *IEEE Trans. Image Processing*, 5(9):1377–1382, 1996.